

An Empirical Investigation of the Forward Interest Rate Term Structure

Andrew Matacz^{1*} and Jean-Philippe Bouchaud^{1,2†}

¹ Science and Finance

109-111 rue Victor Hugo

92632 Levallois, France

<http://www.science-finance.fr>

² Service de Physique de l'Etat Condensé

CEA-Saclay, Orme des Merisiers

91 191 Gif s/ Yvette, France

May 15, 2018

Abstract

In this paper we study empirically the Forward Rate Curve (FRC) of 5 different currencies. We confirm and extend the findings of our previous investigation of the U.S. Forward Rate Curve. In particular, the average FRC follows a square-root law, with a prefactor related to the spot volatility, suggesting a Value-at-Risk like pricing. We find a striking correlation between the instantaneous FRC and the past spot trend over a certain time horizon, in agreement with the idea of an extrapolated trend effect. We present a model which can be adequately calibrated to account for these effects.

1 Introduction

The statistical analysis of the time fluctuations of financial assets is a rapidly growing activity, partly due to the easy access of large quantities of data, and also to the need of finding more adequate models of the behaviour of financial markets. This is important both for risk control purposes, and for a better pricing and hedging of derivative products [1, 2]. The case of the interest curve is particularly interesting and difficult, since one must find a consistent description of the time evolution of a one dimensional *curve* (the interest rate for different

*Email: andrew.matacz@science-finance.fr

†Email: bouchaud@spec.saclay.cea.fr

maturities), rather than that of a single point in the case of a stock or a currency. Interest rate derivatives pricing and hedging, or Asset Liability Management, require an adequate model for the evolution and deformation of the full interest curve [3, 1]. The empirical description of the time variation of the interest curve is therefore very useful for many practical applications.

In a previous paper [4], a series of observations concerning the U.S. forward rate curve (FRC) $f(t, \theta)$ were reported, which are in strong disagreement with the predictions of standard models of interest rates in the literature. The most striking empirical results are the following:

- The average shape of the FRC is well fitted by a square-root law as a function of maturity, with a prefactor very close to the spot rate volatility. This strongly suggests that the forward rate curve is calculated by the money lenders (who dominate the interest rate markets) using a *Value-at-Risk (VaR) like procedure*, and not, as assumed in standard models, through an averaging procedure. More precisely, since the forward rate $f(t, \theta)$ is the agreed value at time t of what will be the value of the spot rate at time $t + \theta$, a VaR-pricing amounts to writing:

$$\int_{f(t, \theta)}^{\infty} dr' P_M(r', t + \theta | r, t) = p, \quad (1.1)$$

where r is the value of the spot rate at time t and P_M is the market implied probability of the future spot rate at time $t + \theta$. The value of p is a constant describing the risk-averseness of money lenders. The risk is that the spot rate at time $t + \theta$, $r(t + \theta)$, turns out to be larger than the agreed rate $f(t, \theta)$. This probability is equal to p within the above VaR pricing procedure. If $r(t)$ performs a simple unbiased random walk, then Eq. (1.1) indeed leads to $f(t, \theta) = r(t) + A(p)\sigma_r\sqrt{\theta}$, where σ_r is the spot rate volatility and $A(p)$ is some function of p .

- There is a strong *positive* correlation between the time variation of the ‘partial spread’ $s(t, \theta) \equiv f(t, \theta) - r(t)$ and the spot rate $r(t)$, which reaches a maximum around $\theta^* = 1$ year and then decreases. Within the standard Vasicek model, this correlation is *negative* and monotonously decreasing with θ . This means that a change in r not only results in a parallel translation of the FRC, but is actually *amplified* around θ^* . Correspondingly, the volatility of the forward rate is found to be ‘humped’ around $\theta^* = 1$ year. This can be interpreted within the above VaR pricing procedure as a time dependent anticipated trend, which is determined by the past historical trend of the spot rate itself over a certain time horizon. In other words, the market looks at the past and extrapolates the observed trend in the future. When the spot rate goes up, the market anticipated trend also typically goes up, and this increase is multiplied by the maturity θ , leading to the above mentioned positive correlation.
- Finally, the decay of the eigenvalues of the deformation correlation matrix for different maturities, as well as some plausible arguments, suggest that the evolution equation for $f(t, \theta)$ contains a second derivative, ‘line tension’ term $\partial_\theta^2 f(t, \theta)$, which tends to

smooth out short wavelengths deformations of the FRC. This term is in general absent in arbitrage free models, but its presence (allowed, for example, by the existence of transaction costs) totally changes the nature of the equation, and has many interesting consequences [4, 5]. Therefore, the search for no arbitrage models might be much too strong a constraint to represent faithfully the empirical behaviour of interest rates.

The aim of the present paper is two fold. First of all, we investigate the empirical behaviour of the FRC of five different currencies (USD, DEM, GBP, AUD and JPY), in the period 1987-1999 for the USD and 1994-1999 for the other currencies. We discuss the similarities and differences between these currencies. The picture drawn from the USD data is, to a large degree, universal. Second, we specify better the interpretation framework sketched in [4], and show how one can calibrate the parameters in a systematic way. We confirm in particular, the rather spectacular correlation between the amplitude of the deformation of the FRC away from its average and the past trend of the spot rate.

2 Data sets and notation

Our study is based on data sets of daily prices of futures contracts on 3 month forward interest rates. These contracts and their exchanges are: the Eurodollar CME-IMM contract, the Short Sterling LIFFE contract, the Euromark LIFFE contract, the Bank Accepted Bills SFE contract and the Euroyen TIFFE contract. In practice, the futures markets price three months forward rates for *fixed* expiration dates, separated by three month intervals. Identifying three months futures rates to instantaneous forward rates, we have available time series on forward rates $f(t, T_i - t)$, where T_i are fixed dates (March, June, September and December of each year), which we have converted into fixed maturity (multiple of three months) forward rates by a simple linear interpolation between the two nearest points such that $T_i - t \leq \theta \leq T_{i+1} - t$. The shortest available maturity is $\theta_{\min} = 3$ months, and we identify $f(t, \theta_{\min})$ to the spot rate $r(t)$. Table 1 gives the time periods and the number of maturities available for each data set. We also have analyzed the data corresponding to the JPY, for which we only have 9 different maturities. This last data set is very similar to the DEM, which appears to be somewhat different than the other currencies, for reasons that we shall discuss below. For empirical studies on intraday Eurofutures data see Piccinato *et-al* [7].

We will define the ‘partial’ spread $s(t, \theta)$, as the difference between the forward rate of maturity θ and the spot rate: $s(t, \theta) = f(t, \theta) - r(t)$. The ‘long’ spread $s(t)$ is simply the partial spread at θ_{\max} : $s(t) = s(t, \theta_{\max})$. The time evolution of $r(t)$ and $s(t)$, for the different data sets is shown in Fig. 1 and Fig. 2.

Since we only have daily data, our reference time scale will be $\tau = 1$ day. The variation of $f(t, \theta)$ between t and $t + \tau$ will be denoted as $df(t, \theta)$:

$$df(t, \theta) = f(t + \tau, \theta) - f(t, \theta). \quad (2.1)$$

	Period	Number of maturities	θ_{\max} (years)
USD 87-99	22/6/87-18/2/99	11	2.75
USD 94-99	1/1/94-18/2/99	38	9.5
GBP	18/3/94-18/2/99	11	2.75
DEM	15/3/94-22/1/99	11	2.75
AUD	17/3/94-18/2/99	11	2.75

Table 1: The datasets

More generally, the difference between the values of any observable $O(t)$ between times t and $t + \tau$ will be noted dO . The theoretical time average of $O(t)$ will be denoted as $\langle O(t) \rangle$. We will refer to empirical averages (over a finite data set) as $\langle O(t) \rangle_e$. For infinite datasets the two averages are the same.

3 Fundamental Empirical Results

The purpose of this section is to present the most important empirical results that are independent of our chosen FRC modelisation. The details of our model and further important empirical results will be discussed in the next 3 sections.

3.1 The average FRC

We consider first the average FRC, which can be obtained from empirical data by averaging the partial spread $s(t, \theta)$:

$$\langle s(t, \theta) \rangle_e = \langle f(t, \theta) - r(t) \rangle_e. \quad (3.1)$$

In Figures 3 and 4 we show the average FRC, $\langle s(t, \theta) \rangle_e$, for the available data sets. As noticed in [4] for the USD case, these average curves can be quite satisfactorily fitted by a simple square-root law, except for the DEM (see the bottom left subfigure of Figure 4). For all these data sets, we also show the following best fit:

$$\langle s(t, \theta) \rangle_e = a(\sqrt{\theta} - \sqrt{\theta_{\min}}). \quad (3.2)$$

The corresponding values of a (in % per $\sqrt{\text{year}}$) are given in Table 2. It is interesting to compare the value of $a/\sqrt{250}$ with the daily volatility of the spot rate, which we shall denote σ_r . For all cases, except for the DEM and the JPY, we find that these two quantities are very close to each other.

We thus fully confirm here – with much more empirical data – the suggestion of ref. [4] that the FRC is on average fixed by a VaR-like procedure, specified by Eq. (1.1) above. The FRC appears to be the *envelope* of the future evolution of the spot rate. If the spot rate

	a	σ_r	$a/\sqrt{250}$
USD 94-99	0.78	0.047	0.049
USD 87-99	1.18	0.067	0.075
GBP	0.91	0.053	0.058
AUD	1.43	0.078	0.090
DEM	1.50	0.033	0.095

Table 2: Parameters for Eq. (3.2). The units for σ_r are % per square-root day.

fluctuates around a reasonable equilibrium value, then the anticipated trend on the spot rate is *on average* zero. The implied probability P_M , appearing in Eq. (1.1) is therefore centered around the present value of the spot rate; this leads to the simple square-root law discussed above.

As will be discussed at length in the next sections, even when the anticipated trend is on average zero, it is not zero for any given day. Its presence leads to much of the interesting effects seen on the deformation of the FRC away from its average shape. There are however, as we discuss now, situations where the average anticipated trend is expected to be non zero.

3.2 Mean reversion effects

As obvious from Figure 4 and Table 2, the DEM data is different. The FRC increases with maturity much faster than it should according to the unbiased VaR procedure explained above. However, a look at Figures 1 and 2 allows one to understand why this might be so. In all the cases, except the DEM, the spot rate is fluctuating around an ‘equilibrium’ rate of about 6.5%. Interest rates are neither too low nor too high and the markets have no reason to expect the future value of the spot rate to move outside a fairly narrow band. On the other hand the DEM spot rate shows a large down trend and the average spot is a low 3.93% (a similar but more extreme situation is seen on the JPY data). It is not in an equilibrium regime, or at least the markets do anticipate a reversion towards higher rates.¹ One might then expect that for ‘short’ time periods, where the spot rate remained low or high on average, the shape function $Y(\theta)$ can effectively be spot dependent. A reasonable guess, inspired from the Vasicek model, is that the partial spread $s(t, \theta)$, evolves about a time dependent mean, given by:

$$s_0(r, \theta) = \sigma_r \left(\sqrt{\theta} - \sqrt{\theta_{\min}} \right) + \left(r_0 - r(t) \right) \left(1 - e^{-\lambda_r(\theta - \theta_{\min})} \right), \quad (3.3)$$

which is the sum of the VaR-like term $\sqrt{\theta}$ and a mean reverting term, characterized by an equilibrium spot rate r_0 and a reversion time $1/\lambda_r$. A consequence of Eq. (3.3) is that the

¹The expectation of a rise of the spot rate might also be due in part to the ‘Euro effect’.

empirical average of the partial spread becomes:

$$\langle s(t, \theta) \rangle_e = \sigma_r \left(\sqrt{\theta} - \sqrt{\theta_{\min}} \right) + \left(r_0 - \langle r(t) \rangle_e \right) \left(1 - e^{-\lambda_r(\theta - \theta_{\min})} \right). \quad (3.4)$$

For $\langle r(t) \rangle_e \simeq r_0$, the mean reversion term is absent, and one recovers the simple $\sqrt{\theta}$ law of Eq. (3.2). In the bottom right of Figure 4 we have found the best fit of $\langle s(t, \theta) \rangle_e$ based on Eq. (3.4). Using the empirical DEM volatility for σ_r , we found $\lambda_r = 0.22$ per year and $r_0 - \langle r \rangle_e = 2.98\%$. Since for the DEM data $\langle r(t) \rangle_e = 3.9\%$, these results imply that the market expects a mean reversion to approximately 7% over a timescale of 5 years. These numbers are very realistic and suggest that Eq. (3.4) qualitatively accounts for the strong anticipated upward trend present in the DEM data. Of course, for datasets long compared to the spot mean reversion timescale, the empirical average reduces to the model average and Eqs. (3.2) and (3.4) are the same. Much the same features are found for the JPY.

3.3 Spread-spot response function and volatility of the FRC

We shall study how a change in the value of the spot rate affects the rest of the FRC, after subtracting the trivial overall translation of the curve. This will define a ‘spread-spot response function’² $\mathcal{R}(\theta)$, through the following dynamical equation:

$$df(t, \theta) = [1 + \mathcal{R}(\theta)]dr(t) + dz(t, \theta), \quad (3.5)$$

where, $dz(t, \theta)$, are spot independent noise increments and we have the constraints:

$$\mathcal{R}(\theta_{\min}) = dz(t, \theta_{\min}) = 0. \quad (3.6)$$

If the response function is positive, then a change in the spot is *amplified* along the FRC. As we discuss below, the response function is, in fact, a more fundamental quantity than the FRC volatility. It determines much of the qualitative shape of the FRC volatility which, itself, is given by a less intuitive contribution of the three terms appearing in Eq. (3.5).

From Eq. (3.5) we find that the response function, $\mathcal{R}(\theta)$, can be measured by computing the empirical average:

$$\mathcal{R}(\theta) = \frac{\langle ds(t, \theta)dr \rangle_e}{\langle dr^2 \rangle_e}. \quad (3.7)$$

In figure 5 we show, for two time periods, the response function for our USD data, while in figure 6 we show the response function for three different currencies, all for the same time period. We see that in all cases, $\mathcal{R}(\theta)$ reaches a positive peak at $\theta = 0.75 - 1$ year, followed by a decay to some negative value. The same features were found for the JPY. This qualitative shape of the response function appears to be rather *universal* across currencies and periods. In figure 9 we show the empirical volatility for the USD, defined as:

$$\sigma(\theta) = \sqrt{\langle df^2(t, \theta) \rangle_e}. \quad (3.8)$$

²here after we call this simply ‘the response function’

We see a strong peak in the volatility at 1 year [1, 6]. For the USD 90-93 inclusive, which is not shown, we find a similar peak though not as strong. In figure 10 we show the empirical volatility for the other currencies. In all cases the volatility shows a steep initial *rise* as the maturity grows. We will demonstrate in the next section that this robust qualitative feature can be traced to the positive peak found for the response function.

While it seems reasonable to expect the response function to become small for longer maturities, it is not *a priori* clear why it should show a robust positive peak around 1 year. This is actually in stark contrast to the Vasicek model [3, 1], where \mathcal{R} is found to be *negative*, and monotonously decreasing. Correspondingly, the volatility is exponentially decaying with maturity. Previously [4] it was proposed that the shape of the response function, and consequently that of the FRC volatility, could be explained by an anticipated trend, calibrated on the past behaviour of the spot. Qualitatively, when the market tries to estimate the implied probability $P_M(r', t + \theta | r, t)$, it looks at the past spot trend over some time horizon and extrapolates this trend into the future. In sections 5 and 6 we will present striking empirical confirmation of this proposal.

4 A Phenomenological Model

Based on our empirical findings [4], we consider the following decomposition of the FRC dynamics:

$$f(t, \theta) = r(t) + s(t)Y(\theta) + y(t, \theta), \quad (4.1)$$

with the following constraints:

$$Y(\theta_{\min}) = y(t, \theta_{\min}) = 0, \quad Y(\theta_{\max}) = 1, \quad y(t, \theta_{\max}) = 0. \quad (4.2)$$

We also impose that:

$$\langle y(t, \theta) \rangle = 0. \quad (4.3)$$

We find from Eq. (4.1) that the average FRC is given by:

$$\langle s(t, \theta) \rangle = \langle f(t, \theta) - r(t) \rangle = \langle s(t) \rangle Y(\theta). \quad (4.4)$$

The function $Y(\theta)$ can therefore, up to a scaling by the average long spread, be interpreted as the average FRC, and can be calibrated to the empirical average FRC discussed in section 3.1. Clearly the ‘deformation process’ $y(t, \theta)$ now describes the fluctuations around the average FRC.

We now turn to a more precise description of the FRC decomposition Eq. (4.1). In order to rationalise the data we propose to think of the evolution of the FRC as driven by three independent noises du, dv and dw , of unit variance:

$$\langle du^2 \rangle = 1, \quad \langle dv^2 \rangle = 1, \quad \langle dw^2 \rangle = 1, \quad (4.5)$$

and

$$\langle du \, dv \rangle = 0, \quad \langle du \, dw \rangle = 0, \quad \langle dv \, dw \rangle = 0. \quad (4.6)$$

These three random factors affect the spot rate, the ‘long’ spread and the deformation as follows. The spot rate is the most important factor which, as will be shown below, also strongly affects the evolution of the deformation $y(t, \theta)$. We define:

$$dr(t) = \sigma_r du, \quad (4.7)$$

where σ_r is the spot rate volatility. Although our results are compatible with more general models for the ‘long spread’, we choose for definiteness the following mean reverting equation:

$$ds(t) = \lambda_s (s_0(r) - s(t)) dt + \sigma_r (\mu du + \nu dv), \quad (4.8)$$

where $s_0(r)$ is the (possibly spot dependent – see subsection 3.2) reversion level and λ_s describes the mean reversion speed. For the measurements described in this paper, however, the precise form of the spot and long spread mean reversion terms are not important since they are in general negligible compared to the noise terms. The coefficient μ measures the influence of the spot rate on the long spread. More precisely:

$$\langle dsdr \rangle = \sigma_r^2 \mu. \quad (4.9)$$

The spread volatility is given by:

$$\langle ds^2 \rangle = \sigma_r^2 [\mu^2 + \nu^2]. \quad (4.10)$$

Using Eqs. (4.9) and (4.10), one can determine the coefficients μ and ν from the data. These coefficients are shown in Table 3. We see from this table and Eq. (4.8) that the long spread evolves mostly independent from the spot, but there is a persistent negative correlation between the spot and long spread. Note also that except for USD 94-99, the spread uses the 2.75 maturity forward rate. For longer maturity spreads we can expect stronger negative correlations. (Figures 5 and 6 for the response function suggest that the negative response grows slowly with maturity.)

As for the ‘deformation process’ $y(t, \theta)$, our analysis of the empirical data leads us to write it as:

$$y(t, \theta) = C(\theta)b(t) + G(\theta)\eta(t), \quad (4.11)$$

	μ	ν
USD 94-99	-0.22	1.17
USD 87-99	-0.18	0.65
GBP	-0.18	1.11
AUD	-0.05	0.99
DEM	0.02	1.22

Table 3: Parameters μ and ν extracted from Eqs. (4.9) and (4.10).

with the constraints:

$$C(\theta_{\min}) = G(\theta_{\min}) = 0, \quad C(\theta_{\max}) = G(\theta_{\max}) = 0. \quad (4.12)$$

The function $b(t)$ is what was called in [4] the ‘anticipated trend’, while $\eta(t)$ is a mean reverting noise term. Due to Eq. (4.3), we require that:

$$\langle b(t) \rangle = \langle \eta(t) \rangle = 0. \quad (4.13)$$

The logic behind Eq. (4.11) is the following: within a VaR-like pricing, the FRC is the envelope of the future anticipated evolution of the spot rate. On average, this evolution is unbiased (provided $r(t)$ is not too far from its equilibrium value r_0), and the average FRC is a simple square-root. However, at any particular time t , the market anticipates a future trend $b(t)$. This means that the probability distribution of the spot, $P_M(r', t + \theta | r, t)$ is not centred around r , but around $r + b(t)\theta$ (for small θ). However, the market also ‘knows’ that its estimate of the trend will not be good on the long run. We therefore write more generally that the distribution is centered around $r + b(t)C(\theta)$.

How does the market determine $b(t)$? One of the main proposals of [4] was that the anticipated trend actually reflects the actual past trend of the spot rate. In other words, the market extrapolates the observed past behaviour of the spot to the nearby future. More precisely, we write:

$$b(t) = \int_{-\infty}^t K(t - t') dr(t'), \quad (4.14)$$

where K is an averaging kernel, which we normalize such that $K(0) = 1$. We have considered two choices for $K(u)$: an exponential form, which leads to an Ornstein-Uhlenbeck (OU) process for b driven by the spot rate $r(t)$,

$$db(t) = -\lambda_b b(t) dt + dr(t), \quad (4.15)$$

or a simple flat window (FW) of width T_b , leading to:

$$b(t) = r(t) - r(t - T_b). \quad (4.16)$$

At this stage, the model has only two factors: the spot rate, and the noise term dv driving the long spread. It is clear that since the long term extrapolation of the anticipated trend is doubtful, one should also add an extra noise term $G(\theta)\eta(t)$ to $r + b(t)C(\theta)$, where the ‘signal to noise’ ratio $C(\theta)/G(\theta)$ should become small for large θ ’s. For the noise term $\eta(t)$ we also propose a simple mean reverting (OU) process driven by our third factor dw :

$$d\eta(t) = -\lambda_\eta \eta(t) dt + \sigma_r dw. \quad (4.17)$$

We have thus assumed that the deformation is driven by the spot and a noise. Because the noise dw has been scaled by σ_r , we can directly compare the functions G and C . By comparing them we can see how much of the deformation is driven by the spot compared to noise. The model assumption in (4.17) is that the deformation noise is furthermore

independent of the long spread noise. Eq. (4.17), together with the preceding equations, fully defines our three factor model.

In our model the response function is given by:

$$\mathcal{R}(\theta) = \frac{\langle ds(t, \theta) dr \rangle}{\langle dr^2 \rangle} = \mu Y(\theta) + C(\theta). \quad (4.18)$$

Note that for θ_{\max} , this equation is identical to Eq. (4.9) above. From the previous knowledge of $Y(\theta)$ and μ , we can calibrate $C(\theta)$ to our empirical response function, $\mathcal{R}(\theta)$, discussed in section 3.3. The results are shown in Figures 7 and 8. We again find a robust positive peak at $\theta = 0.75 - 1$ year which is due to the same positive peak found in figures 5 and 6 for the response function.

Neglecting the contribution of all drifts, the square of the maturity dependent volatility of the forward rates read, within our theoretical framework:

$$\begin{aligned} \sigma^2(\theta) &= \sigma_r^2 \left[1 + 2C(\theta) + 2\mu Y(\theta) + Y^2(\theta)(\mu^2 + \nu^2) \right. \\ &\quad \left. + 2\mu Y(\theta)C(\theta) + Q_K C^2(\theta) + G^2(\theta) \right], \end{aligned} \quad (4.19)$$

where $Q_K = 1$ when the averaging kernel defining $b(t)$ is taken to be exponential, and $Q_K = 2$ if it is taken to be flat. For θ_{\max} , this equation reduces to the previous Eq's (4.9,4.10). The only unknown left to calibrate using this equation is the noise contribution to the deformation, $G(\theta)$.

In Figs. 9 and 10 we plot the empirical volatility and the square root of Eq. (4.19) when $C = G = 0$ and also when $G = 0$. In this section we have chosen to use the value $Q_K = 2$ since this leads to a higher signal to noise ratio. Another justification of this choice will be given in the next section. For the former case, the deformation has been set to zero, and the model has only been calibrated to the spot, the long spread volatility and the average FRC. In the latter case the model is also calibrated to the response function which includes the effect of the proposed anticipated bias (but not the 3rd noise factor). The empirical FRC volatility was discussed in section 3.3 where we emphasized the universal steep initial rise in the volatility with increasing maturity. We can now see that the response function, and consequently the proposed anticipated bias, make a large contribution to the FRC volatility and, in fact, seem to be responsible for the universal step rise in the FRC volatility function. Using Eq. (4.19), we can calibrate $G(\theta)$ to the empirical volatility shown in Figs. 9 and 10. The signal to noise ratio $C(\theta)/G(\theta)$ is plotted in Figure 11 for the different currencies. It is seen to decrease monotonously with θ , in accordance with our interpretation of $C(\theta)$ as an extrapolated trend contribution, the influence of which is bound to decay with maturities.

We have chosen to describe the FRC using three (correlated) components that have a direct financial interpretation: the spot, long spread and deformation. It is useful to compare the volatility and kurtosis of these three components. For the deformation, we consider the 1 year maturity, corresponding to the maximum amplitude of this component. We show the results in Table 4 below. It is interesting to see the high kurtosis of all components and the

	σ_r	σ_s	σ_y	k_r	k_s	k_y
USD 94-99	0.047	0.051	0.035	6.6	6.9	8.4
USD 87-99	0.067	0.045	0.028	37.8	9.7	6.2
GBP	0.053	0.059	0.029	5.9	10.6	12.9
AUD	0.078	0.078	0.028	8.0	6.4	5.6
DEM	0.033	0.040	0.028	5.5	3.2	4.3

Table 4: Daily volatility and kurtosis of the spot, long spread and deformation (1 year maturity) for the datasets. The volatility units are % per square-root day.

relative stability of the deformation volatility across the different datasets. Even though the long spread volatility is greater than the deformation volatility, the deformation remains the more important component at the short end of the FRC. This follows because of the function $Y(\theta)$ goes to zero for short maturities (see Eq. (4.1)).

5 Direct Confirmation of the Anticipated Trend

Both in [4] and in the previous section, the anticipated trend, defined by Eq. (4.14), was proposed as an explanation of the robust positive peak in the response function, Eq. (4.18). We also saw that the anticipated trend could explain the qualitative shape of all the FRC volatility functions as well as the decay in the signal to noise ratio. However, although this empirical evidence is compelling, it does not constitute the most direct empirical confirmation of the anticipated trend. This is because all the previous measurements are increment based and not directly sensitive to the memory timescale of the averaging kernel in Eq. (4.14).

To more directly confirm the anticipated trend mechanism, we need to study the empirical deformation process itself rather than the FRC increments. The empirical deformation process is easily extracted from the data using:

$$y(t, \theta) = f(t, \theta) - r(t) - s(t)Y(\theta). \quad (5.1)$$

By construction it is zero at the endpoints and also has zero mean. In our current 3 factor formulation, our model deformation is described by Eq. (4.11) where we consider Eq's. (4.15) and (4.16) as possible models for the anticipated trend $b(t)$, and Eq. (4.17) as a simple model for the noise component. We saw in the previous section how the functions $C(\theta)$ and $G(\theta)$ can be calibrated using the response function, Eq. (4.18), and the volatility, Eq. (4.19). To determine the model parameters λ_η and T_b or λ_b , we propose to measure the following average error:

$$\sqrt{\langle (y(t, \theta) - C(\theta)b(t))^2 \rangle} = G(\theta)\sqrt{\langle \eta^2(t) \rangle} = \frac{G(\theta)\sigma_r}{\sqrt{2\lambda_\eta}}, \quad (5.2)$$

which follows from Eq's. (4.11) and (4.17). To measure the LHS of the above equation (the average error), we must first extract the empirical deformation $y(t, \theta)$ using Eq. (5.1). We then determine $b(t)$ using the empirical spot time series and Eq. (4.15) or (4.16).³ The LHS of Eq. (5.2) will have a minimum error for some T_b or λ_b . This is the timescale where the deformation and anticipated trend match up best, thereby fixing the values of T_b or λ_b . We can then use the magnitude of this minimum error to fix λ_η via Eq. (5.2).

Consider first the flat window model, Eq. (4.16) (FW model). In Figure 12 we plot the LHS of Eq. (5.2) for USD 94-99, against the parameter T_b , used in the simulation of $b(t)$. We consider the first 4 maturities beyond the spot-rate. As T_b becomes small, the anticipated trend becomes negligible compared to the deformation in the LHS of Eq. (5.2). In this limit the % error in Figure 12 reduces to the deformation root mean square deviation. Let us first assume that the market believes that the past spot trend contains no useful information about the future spot-rate - in other words, the market believes in the efficient market hypothesis. In this case the deformation process should be uncorrelated with the anticipated trend. This in-turn implies that the LHS of Eq. (5.2) should increase with T_b . In fact, what one sees is a deep minimum indicating the clear presence of a dynamical timescale around 100 days. This demonstrates that the deformation and anticipated trend are strongly correlated. In Figure 13 we plot the empirical deformation against $C(\theta)b(t)$, where we have set $T_b = 100$ days. Indeed, we visually confirm a striking correlation, even out to the 15 month maturity. In Figure 14 we plot the LHS of Eq. (5.2) for the GBP, DEM and AUD case as a function of T_b . We again find minima at 175, 100 and 130 days respectively. In these cases the minima are not so deep which makes the timescale not as well defined as in the USD case. In Figure 15 we plot for the GBP, DEM and AUD, the deformation, $y(t, \theta)$, against $C(\theta)b(t)$, for $\theta = 6$ months. We again see a clear correlation though the quality is not as good as for the USD 94-99 case. This was expected since the signal to noise ratio C/G is smaller in these cases. However the same qualitative features are present for all datasets.

Using Eq. (5.2) we can now estimate λ_η . We use the value of the maturity θ such that $G(\theta)$ is maximum: $\theta = 3$ years for the USD 94-99 data and $\theta = 1.25$ years for other currencies. The values of the different time scales (in trading days) are reproduced in Table 5. As a rule of thumb we can say that the deformation dynamics is mean reverting on a time scale of $\simeq 6$ months. It must be emphasized that these results do not constitute a statistical validation of the drift term in, Eq. (4.17), for the deformation noise. The mean reverting nature of this model was proposed in relation to the existence of a second order derivative term in the evolution of the FRC, discussed in [4, 5]. The specific results obtained for λ_η are only meaningful if the mean reversion assumption is correct.

We have performed an identical analysis using the OU model for the anticipated trend. We find the same optimal timescales as for the FW model. We find that the minimal errors for the GBP and AUD are larger for this model, the error for the DEM is similar but the error for the USD is less (by about 20%). Even though the USD error is less within a OU model, overall we prefer the FW model in a three factor setting for the following reasons:

³In this empirical determination of $b(t)$ we actually use detrended spot increments, defined as $d\hat{r}(t) = dr(t) - \langle dr \rangle_e$.

	T_b	λ_η^{-1}
USD 94-99	100	151
GBP	175	169
AUD	130	114
DEM	100	104

Table 5: Table of the memory time T_b for the FW trend model (4.16) and the noise mean reversion time extracted from Eq. (5.2). The units are trading days.

- It leads to deeper minima and therefore to a better defined optimal timescale
- More significantly, the contribution to the FRC volatility of the anticipated trend is higher, through the factor Q_K defined in Eq. (4.19). This in turn reduces the value of $G(\theta)$ which then increases the signal to noise ratio. For the USD case the reduction of G is rather high for the early maturities. This point is significant because it means we are much better able to simultaneously fit the FRC volatility and response function by $C(\theta)$ alone.
- From Eq. (5.2), a smaller $G(\theta)$ then leads to a larger mean reversion timescale for the noise. For the USD data the OU model gives $\lambda_\eta^{-1} \simeq 50$ days for the first 4 maturities – somewhat lower than that obtained for the FW model.
- Once the optimal T_b has been obtained using the above method, it is interesting to calibrate $C(\theta)$ such that the LHS of Eq. (5.2) is minimal. This of course means that we do not try *a priori* to fit the response function exactly. We find that this method does not lead to any significant reduction of the error. This is a further nice feature of the FW model: the function $C(\theta)$ obtained from the response function also seems to give the optimal fit to the deformation.

6 Reducing the Number of Factors

For the USD 94-99 case, the high signal to noise ratio shown in Fig. 11 suggests that the short end of the FRC could be rather well modelled by a simpler one or two-factor version of our model. One way to obtain the latter is by simply setting $G(\theta) = 0$. In these cases we can not calibrate our model to both the response function, Eq. (4.18), and the volatility, Eq. (4.19). Since the volatility is generally the more important quantity for applications, we choose here to calibrate $C(\theta)$ directly to Eq. (4.19) with $G(\theta) = 0$. In the previous section we calibrated $C(\theta)$ to the response function. In this case the result obtained is independent of our choice of model for the anticipated trend. This is no longer the case when we calibrate $C(\theta)$ to the volatility. Using this calibration procedure for the USD 94-99, it turns out that

the match between the deformation and anticipated trend, for the FW model, is similar to that obtained in section 5. On the other hand we find the match is improved when we use the OU model for the anticipated trend.

In Table 6 below, we compare $C(\theta)$ fitted to the response function (as in the previous sections) and $C(\theta)$ fitted using the volatility in the two-factor version of our model, where we have now chosen the OU model for the anticipated trend. We also compare the minimum errors (at 100 days) for the previous FW model and now for the OU model using the new values for $C(\theta)$. For the OU model a plot similar to Figure 12 shows again a minimum at $\lambda_b^{-1} = 100$ days.

In Figure 16 we plot both the deformation and anticipated trend using the OU model. The correlation is quite spectacular and completely validates the anticipated trend proposal. Clearly, when the signal to noise ratio is high the two-factor version is an excellent model of the FRC deformation. This two-factor model is not as effective for the other currencies since the signal to noise ratio is worse.

For the USD 94-99 data set, not only is the signal to noise ratio much higher than for the other currencies, but the signal to noise ratio persists for longer maturities. From Figure 11 we see that the 2.25 years maturity forward rate has a signal to noise ratio of $\simeq 0.5$. For the other currencies this occurs at approximately the 0.75 year maturity. In Figure 17 we plot the deformation and trend for the 2.25 year (27 months) maturity for both our three-factor and two-factor models. The strong correlation is clearly seen to persist even beyond 2 years forward of the spot!

For the USD 94-99 case, it is important to note that even the one factor version of our model provides a very good description of the deformation about the average curve at the short end. The one factor version of our model is simply:

$$f(t, \theta) = r(t) + a(\sqrt{\theta} - \sqrt{\theta_{\min}}) + \mathcal{R}(\theta)b(t) \quad (6.1)$$

where $a \simeq \sigma_r$ and $\mathcal{R}(\theta)$ is the response function. However, as before, we may prefer to calibrate $\mathcal{R}(\theta)$ to the volatility which now takes the form:

$$\sigma^2(\theta) = \sigma_r^2 [1 + 2\mathcal{R}(\theta) + Q_K \mathcal{R}^2(\theta)]. \quad (6.2)$$

	$C(\theta)$ (3 fac.)	$C(\theta)$ (2 fac.)	Err – FW 3 fac.	Err – OU 2 fac.
6 months	0.32	0.36	0.10	0.074
9 months	0.48	0.55	0.16	0.11
12 months	0.50	0.61	0.17	0.12
15 months	0.48	0.60	0.16	0.12

Table 6: Comparing the fit to the deformation for the 3 factor and 2 factor models. For the USD 94-99.

This model works very well at the short end because, for the early maturities, the spot trend contribution is much greater than the long spread contribution in setting the FRC. This point is particularly important since the short end of the curve is the most liquid part of the curve, corresponding to the largest volume of trading (in particular on derivative markets). Interest rate models have evolved towards including more and more factors to get better models. Yet our study suggests that after the spot, it is the *spot trend* which is the most important model component.

It is important to understand if the popular HJM framework [8] can capture the qualitative features of the simple model Eq. (6.1). Significantly, it seems clear to us that our empirical results for the average FRC cannot be naturally accounted for in this framework. For the one-factor HJM model, the relation between the volatility and response function is the same as Eq. (6.2), when $Q_K = 1$. Empirically we find that a better simultaneous fit of the volatility and response function is obtained when $Q_K = 2$. What is more important but less clear, is whether the HJM framework captures the striking spot trend effect observed. The problem here is that the complexity of the HJM framework does not allow us to easily see how the spot rate drives the forward rates. On the other hand, our model is very close in spirit to the strong correlation limit of the ‘two-factor’ spot rate model of Hull-White [9], which was introduced in an *ad hoc* way to reproduce the volatility hump. Although phrased differently, this model assumes in effect the existence of an extrapolated trend following an OU process driven by the spot rate. In the one-factor perfect correlation limit of this model, we can show that up to negligible σ^2 terms, the model leads to:

$$f(t, \theta) = r(t) + b(t)\mathcal{R}_{HW}(\theta), \quad (6.3)$$

where $b(t)$ is given by Eq. (4.15), while $\mathcal{R}_{HW}(\theta)$ is obtained explicitly as:

$$\mathcal{R}_{HW}(\theta) = \frac{\lambda_r}{\lambda_r - \lambda_b} \left(e^{-\lambda_b \theta} - e^{-\lambda_r \theta} \right). \quad (6.4)$$

One can check that $\mathcal{R}_{HW}(\theta)$ is positive and has a correct qualitative shape, growing linearly for small maturities and decaying to zero for large maturities. This ‘Hull-White II’ model however fails to capture the $\sqrt{\theta}$ behaviour of the average FRC. We furthermore believe that our analysis gives a rather compelling financial interpretation of their model.

7 Discussion and conclusion

In this paper, we analyzed in detail the empirical properties of the forward rate curve corresponding to different currencies. We proposed a theoretical framework to account for the observed properties which builds upon the intuitive picture proposed in [4], and showed in detail how the different parameters entering the model can be calibrated using historical data. The main conclusions of our work are the following:

- The average FRC indeed follows a simple square-root law, with a prefactor closely related to the spot volatility. This strengthens the idea of a VaR-like pricing of the

FRC proposed in [4]. When the spot rate is very low (or very high) compared to its historical average, this square-root law fails to describe the data. One can indeed expect a strong average anticipated mean reversion contribution in these cases. This allows to rationalize our findings on the DEM (and JPY) data.

- The FRC is strongly correlated with the past trend observed on the spot rate. This is strikingly illustrated in Figures 13, 16 and 17 for the USD data, where one sees that the past trend on the spot tracks very closely the amplitude of the FRC deformation. This correlation allows us to account for the strong positive response function and for the volatility hump.
- After the spot, it seems that the *spot trend* is the most important component for modeling the FRC.

It is important to understand whether the popular HJM framework can describe the above observed empirical properties. We feel that our empirical results for the average FRC cannot be naturally accounted for in this framework. For the spot trend effect the situation is less clear. From the empirical evidence presented here, it is clear that this term should be included in any model of the FRC. This offers the interesting possibility of strongly constraining the set of reasonable HJM models. We know of only one spot-rate model that does, in effect, include a spot trend term. This is the strong correlation limit of the Hull-White two-factor model [9]. However, the precise relation, if any, between this model and the HJM framework is unclear and needs to be understood. For work in this direction see Chiarella and Kwon [10].

It would be interesting to understand from first principles the shape of the basic object responsible for the FRC deformation, namely the function $C(\theta)$ which, at the short end, is mainly determined by the response function. A reasonable fit is [4] $C(\theta) = c\theta \exp(-\gamma\theta)$ (see also (6.4) above). The initial linear rise is related to the interpretation of $C(\theta)b(t)$ as an extrapolated trend; the following exponential decay reflects how the market perceives the persistence of this trend over time. Interestingly, a very similar shape for the structure of the deformation was proposed recently by R. Cont [5], based on the diagonalisation of an evolution operator for the FRC which includes a second-order, line tension term, first proposed in [4]. The precise relation – if any – between this two view points needs to be clarified.

A natural extension of our work is to adapt the general method for option pricing in a non-Gaussian world detailed in [2] to interest rate derivatives. Work in this direction is in progress.

Acknowledgements:

We thank J. P. Aguilar, P. Cizeau, R. Cont, O. Kwon, L. Laloux, M. Meyer, A. Tordjman and in particular M. Potters for many interesting discussions.

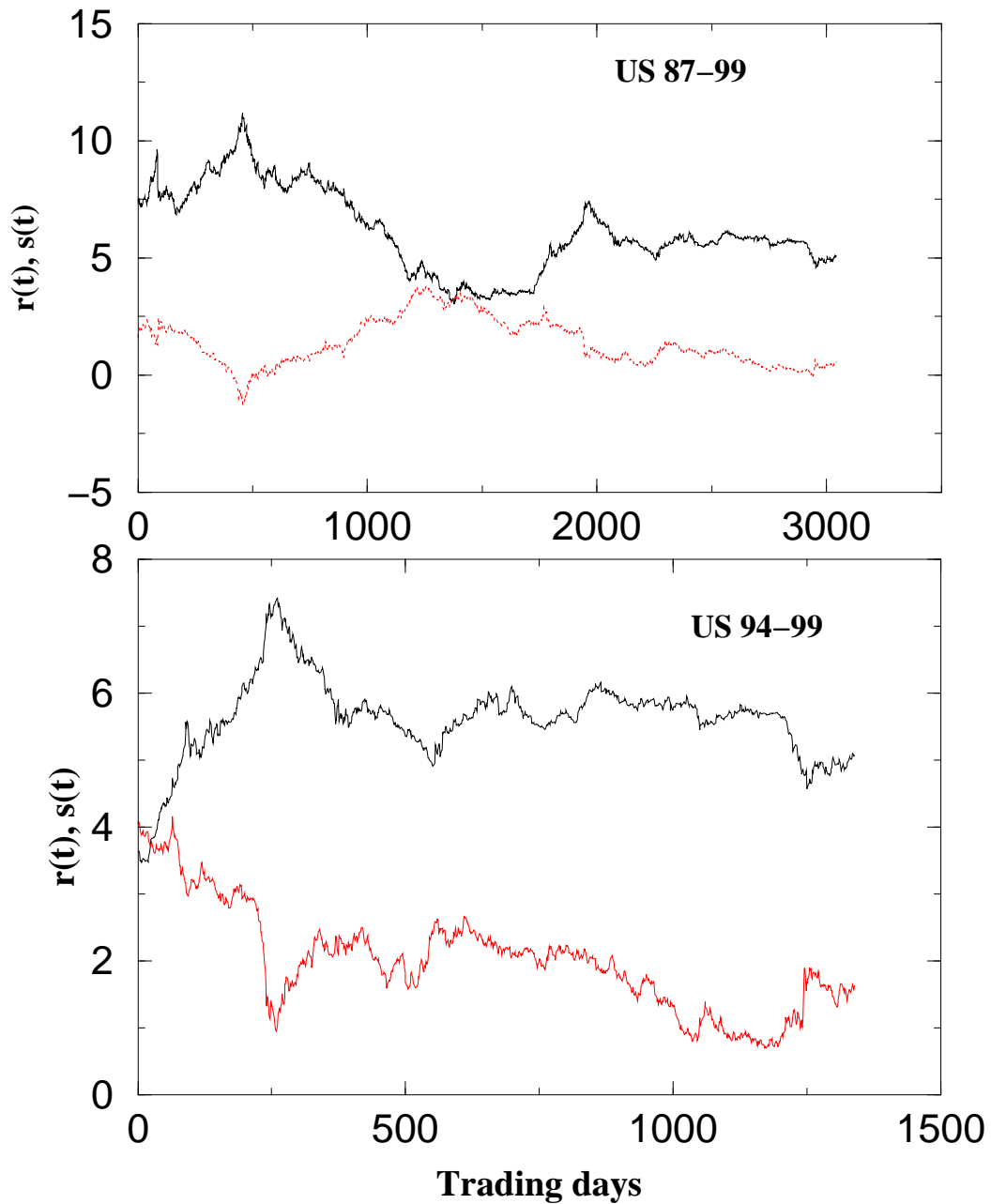


Figure 1: Top Figure: The historical times series of the spot rate (top bold curve) and long spread for our USD 87-99 dataset. Bottom Figure: The same as before but now the dataset is the USD 94-99. For this later case the long spread is defined using the maximum forward rate of 9.5 years, while for the former it is 2.75 years.

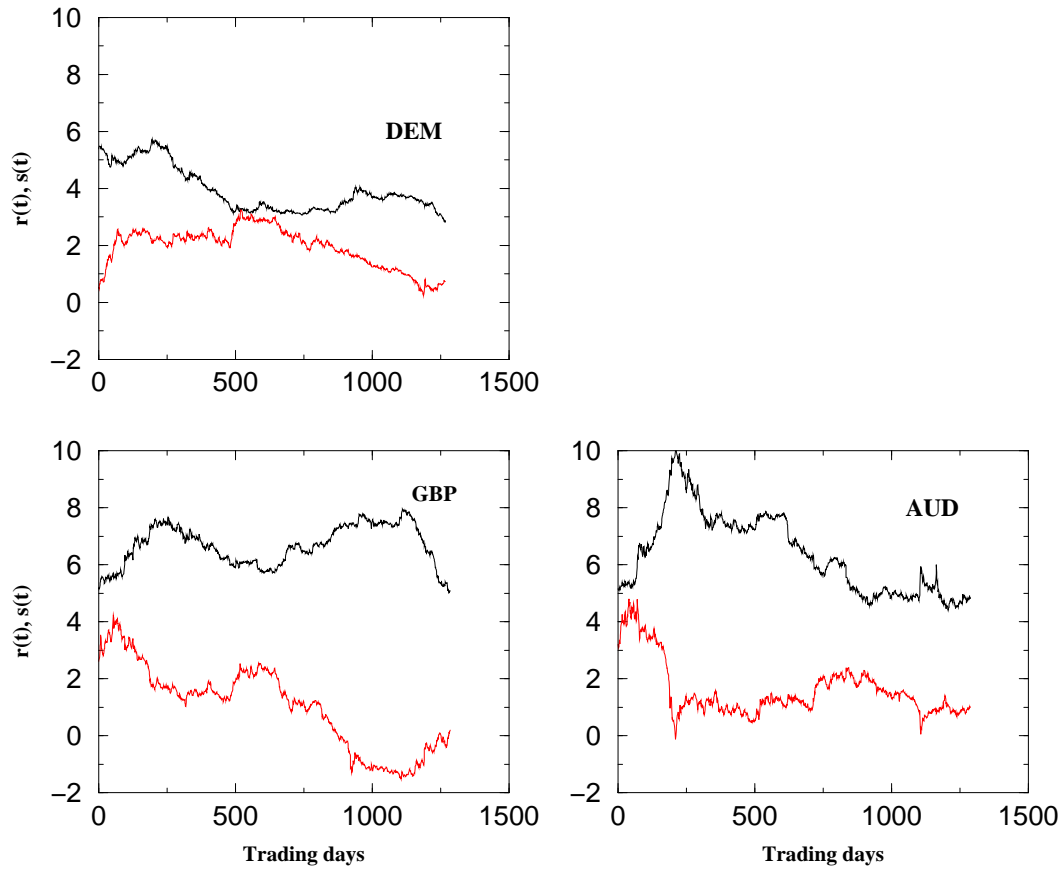


Figure 2: The historical times series of the spot rate (top bold curves) and long spread for the DEM, GBP and AUD. For these cases the long spread is defined using the maximum forward rate of 2.75 years.

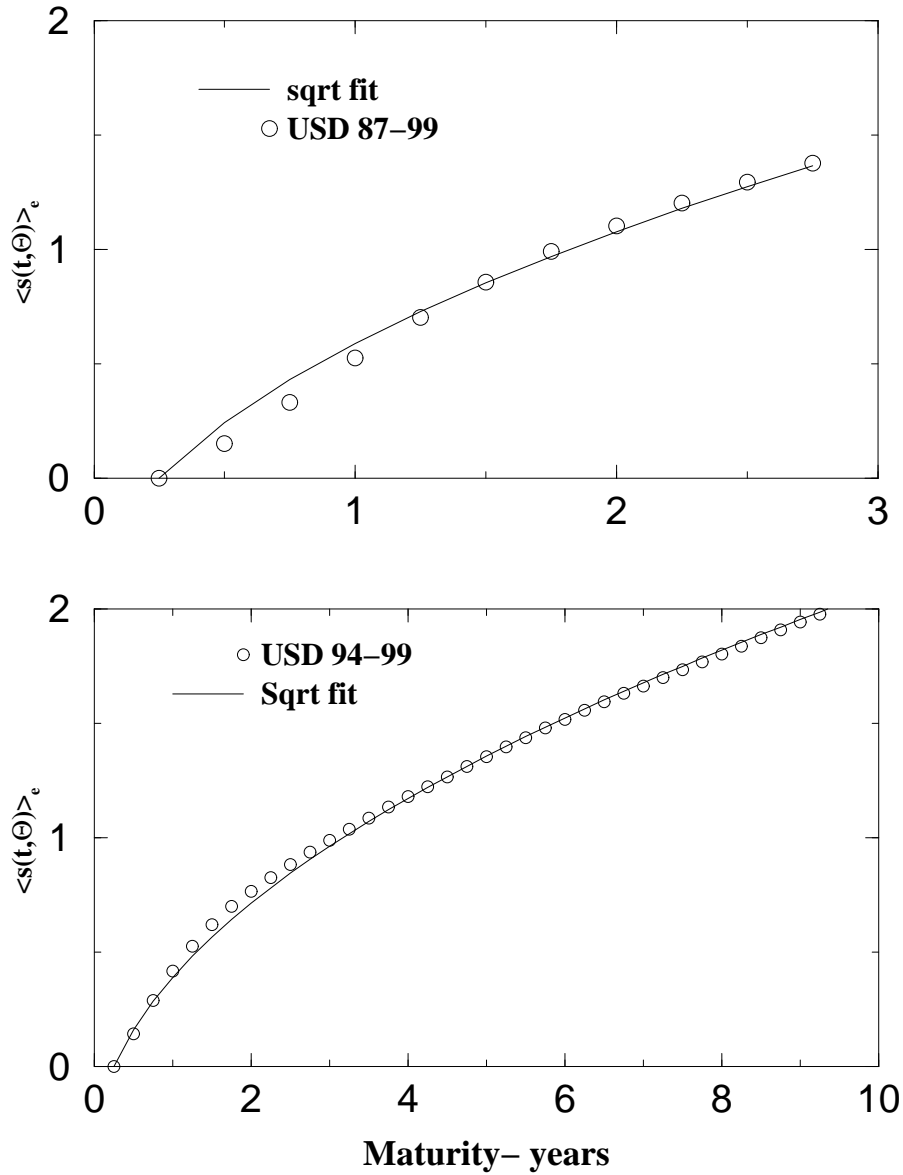


Figure 3: Top Figure: the average FRC in % for USD 87-99, given empirically by Eq. (3.1), and a best fit to Eq. (3.2). The fitting parameter a , is shown in Table 2. Bottom Figure: the same but now for USD 94-99. These figures, along with Table 2, demonstrate that the USD average FRC is well fitted by a square-root law with a prefactor given approximately by the spot volatility.

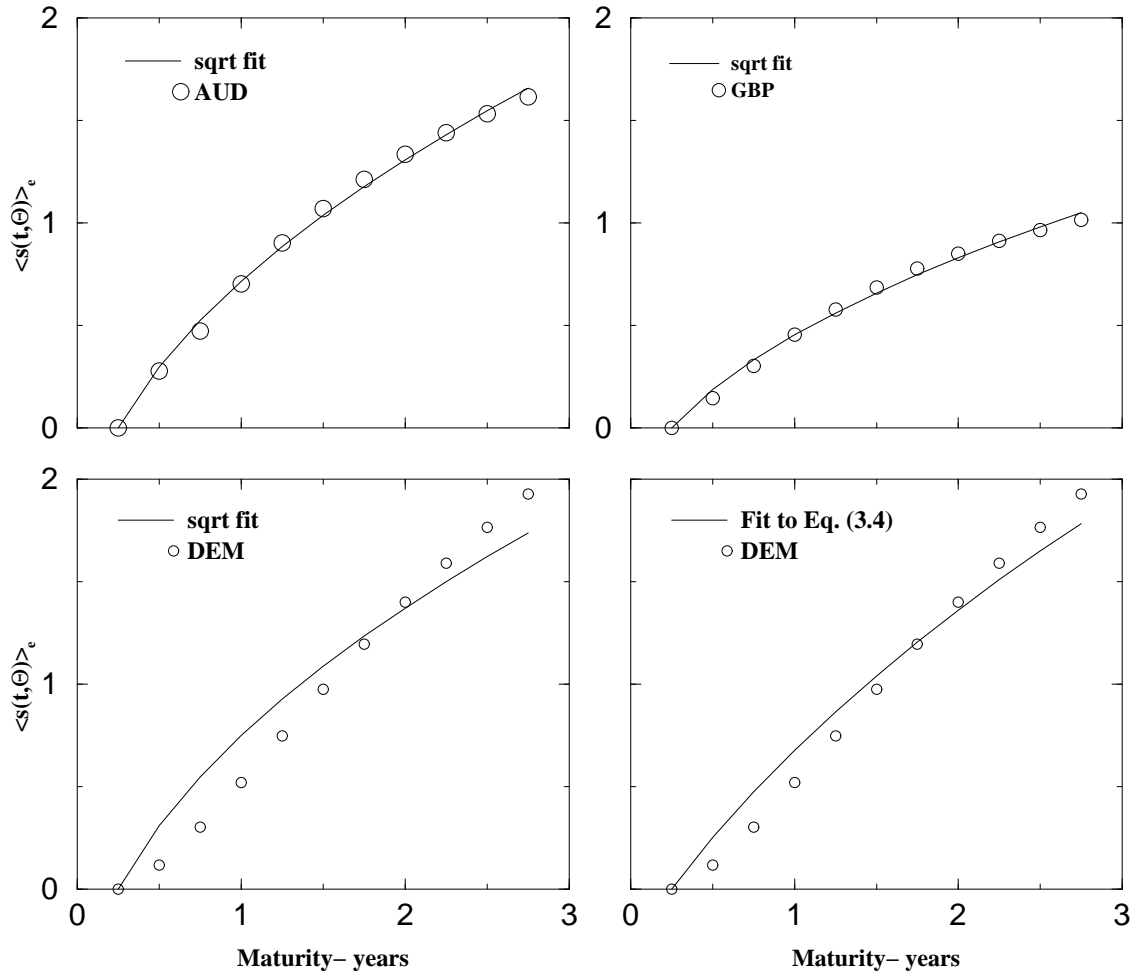


Figure 4: Top left: the same as figure 3 but now for AUD. Top right: the same but now for GBP. Bottom left: the same but now for DEM. Bottom right: here we show the same empirical DEM average FRC, but now with a best fit to Eq. (3.4) rather than Eq. (3.2). These figures, along with Table 2, demonstrate that the AUD and GBP average FRC's are also well fitted by a square root law with a prefactor given approximately by the spot volatility. In section 3.2 we explain why the DEM average FRC cannot be well fitted by a square-root law.

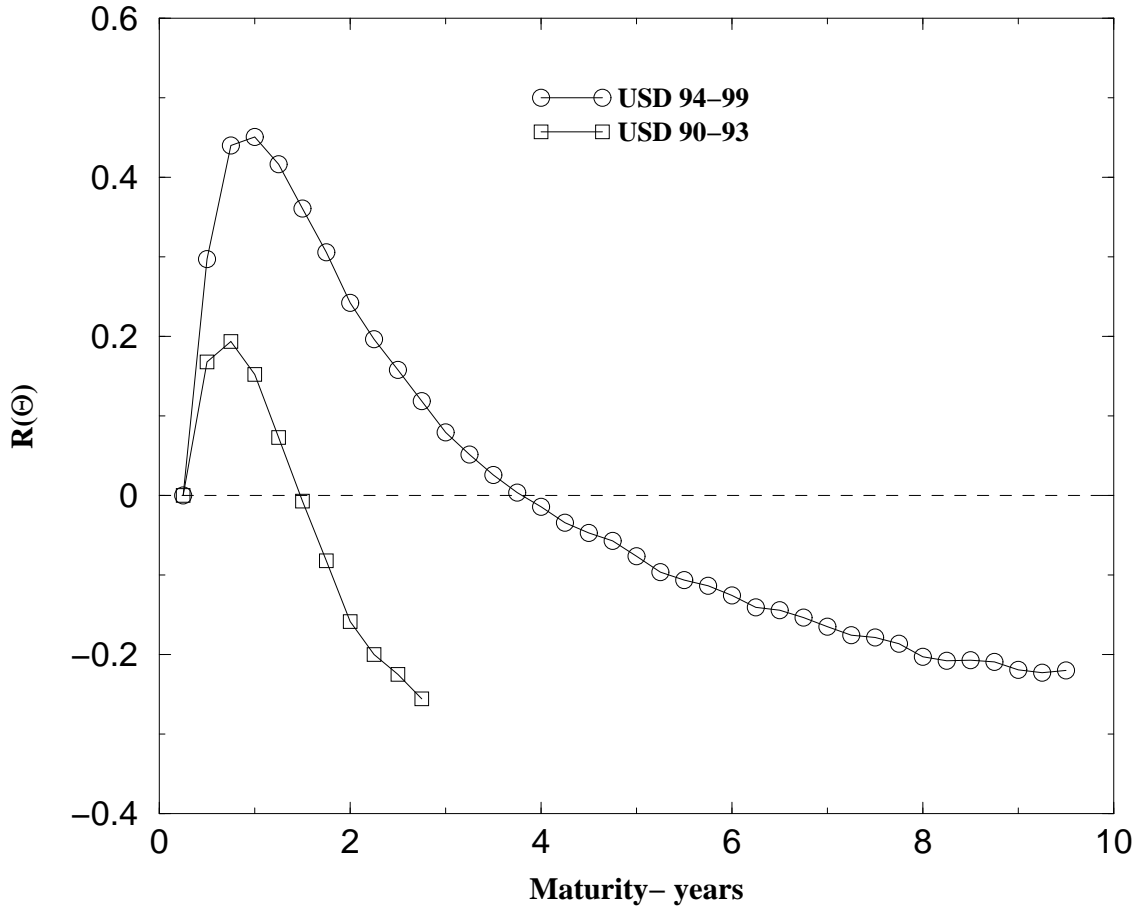


Figure 5: The USD response function, derived empirically from Eq. (3.7). We show results for the dataset USD 94-99 and the 4 year dataset USD 90-93. This figure demonstrates a positive peak at a maturity of 0.75-1 year.

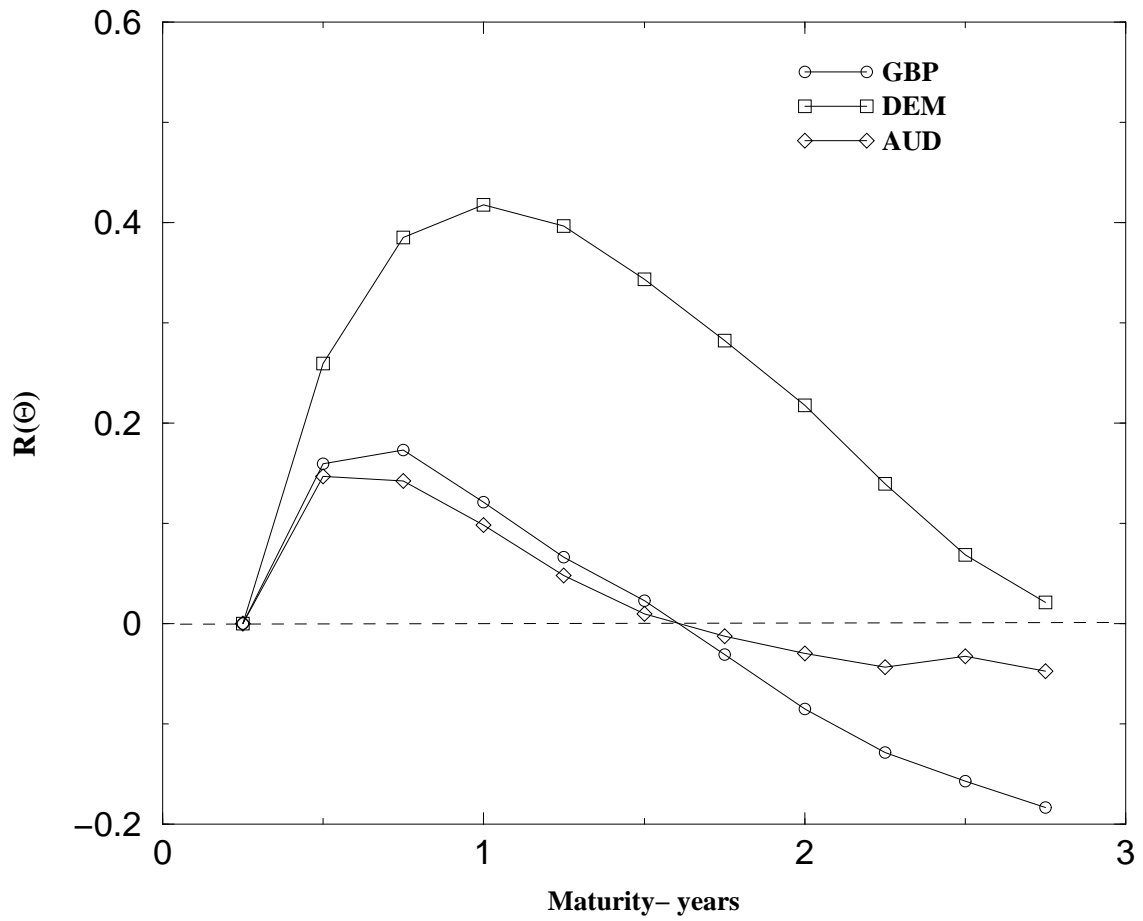


Figure 6: The same as figure 5 but now for GBP, DEM and AUD. This figure demonstrates that the positive peak found in figure 5 is robust across currencies as well as time periods.

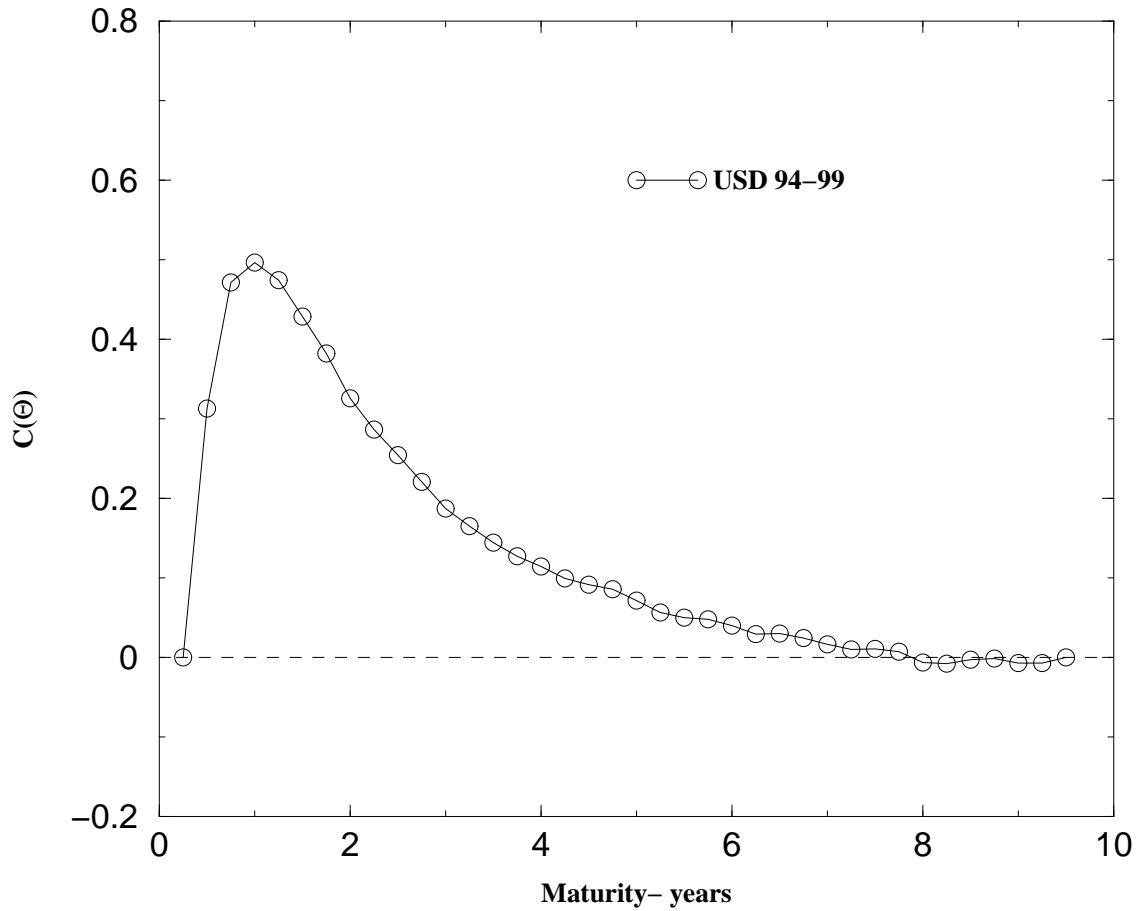


Figure 7: The anticipated trend scaling function, $C(\theta)$, defined in Eq. (4.11), for the USD 94-99. This function is simply deduced from Eq. (4.18), using previous empirical results for the response function and the average FRC. The shape of this function is a consequence of the positive peak shown in figure 5 for the response function.

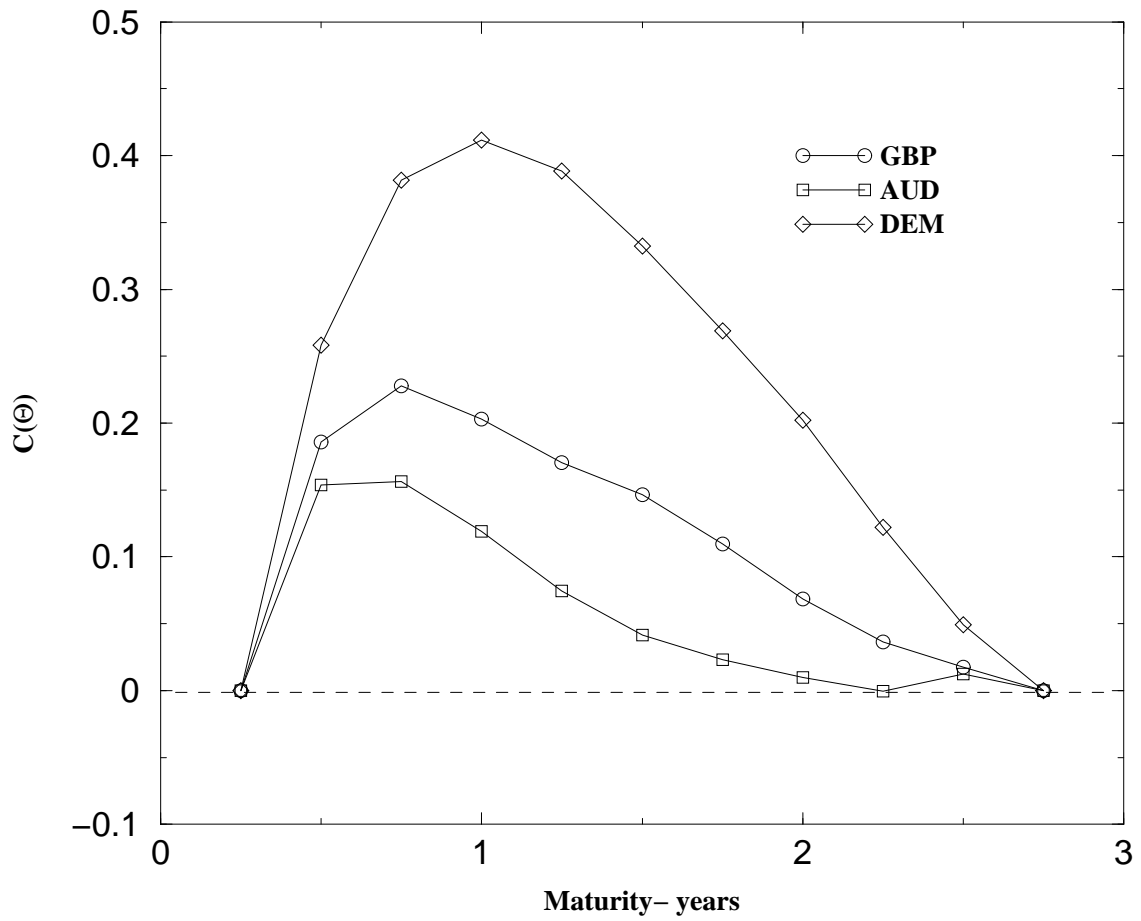


Figure 8: The same as figure 7 but now for GBP, DEM and AUD. Again, the shape of these functions are a consequence of the positive peaks shown in figure 6.

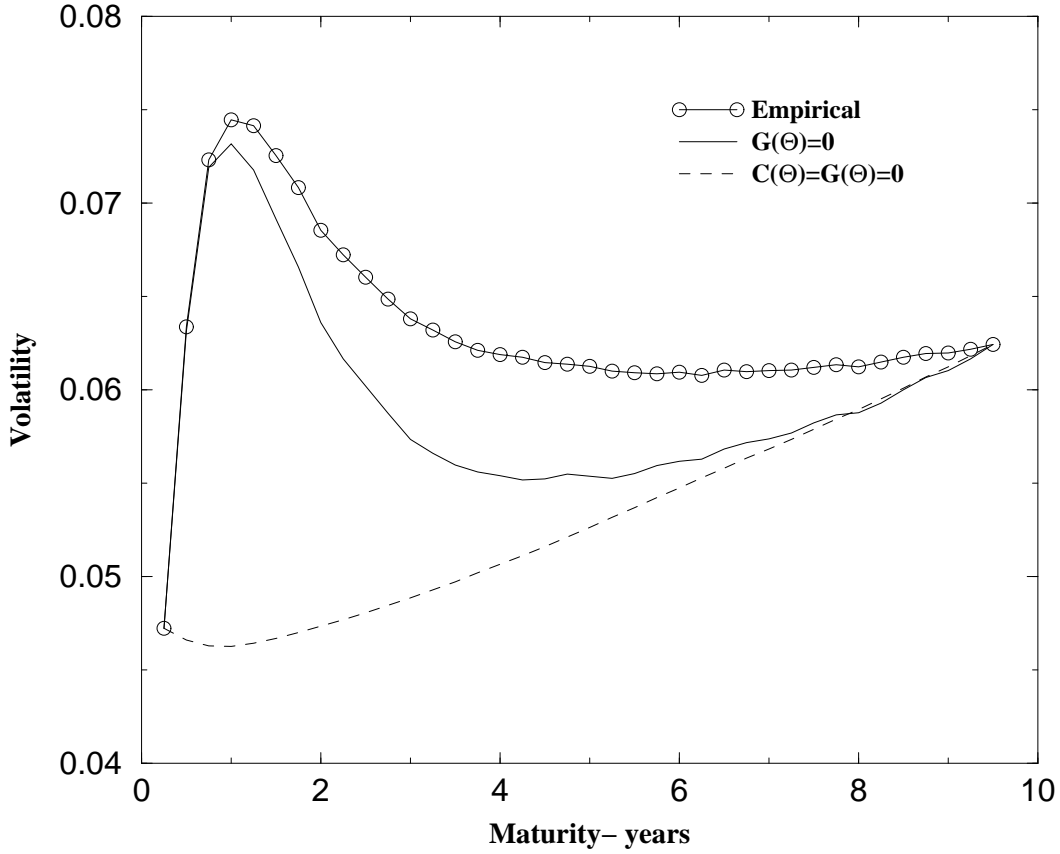


Figure 9: FRC volatility for USD 94-99 in units of % per square-root day. We show the empirical and model volatilities. The empirical volatility is given by Eq. (3.8). The model volatilities are given by the square-root of Eq. (4.19) when $C = G = 0$ and $G = 0$. We have used $Q_K = 2$. In the former case the model has only been calibrated to the spot and long spread volatility and the average FRC. In the latter case the model is also calibrated to the response function. The figure demonstrates how the response function determines the qualitative shape of the FRC volatility.

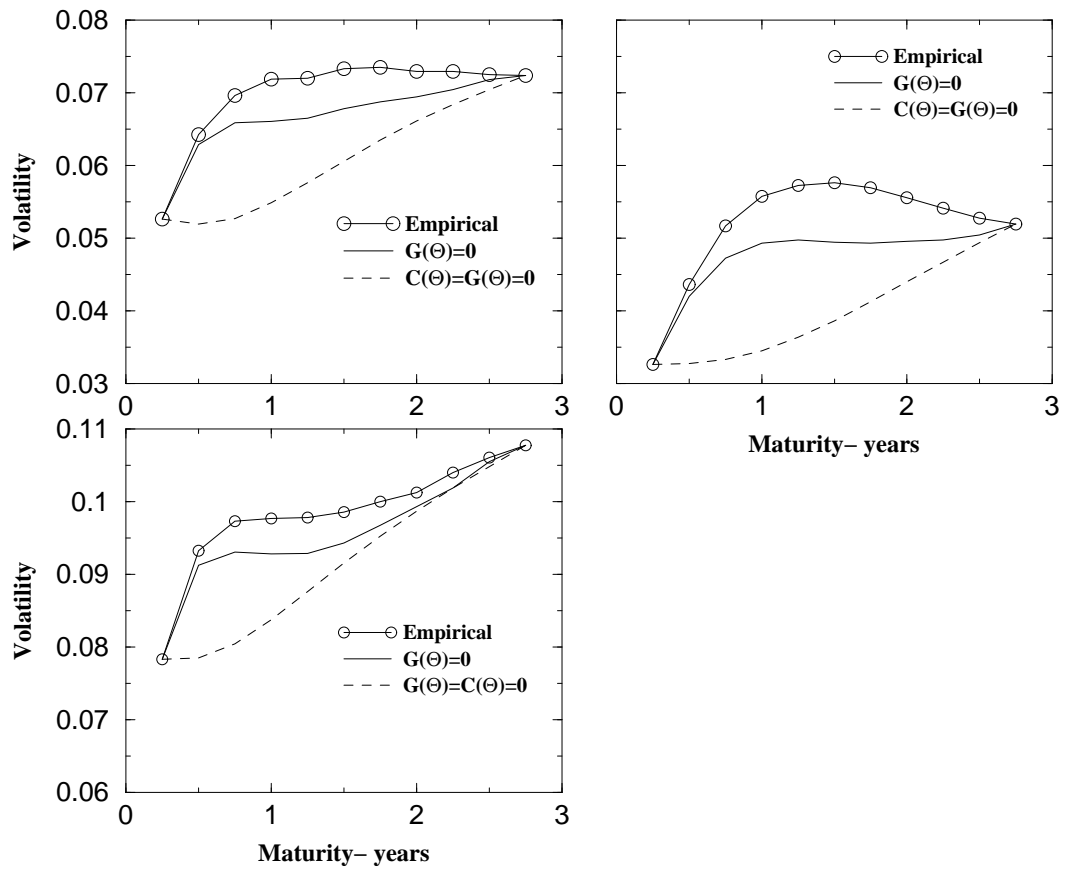


Figure 10: Same as for Figure 9 but now for GBP (top left), DEM (top right) and AUD (bottom left). This figure demonstrates that for all the currencies, the response function determines the qualitative shape of the FRC volatility.

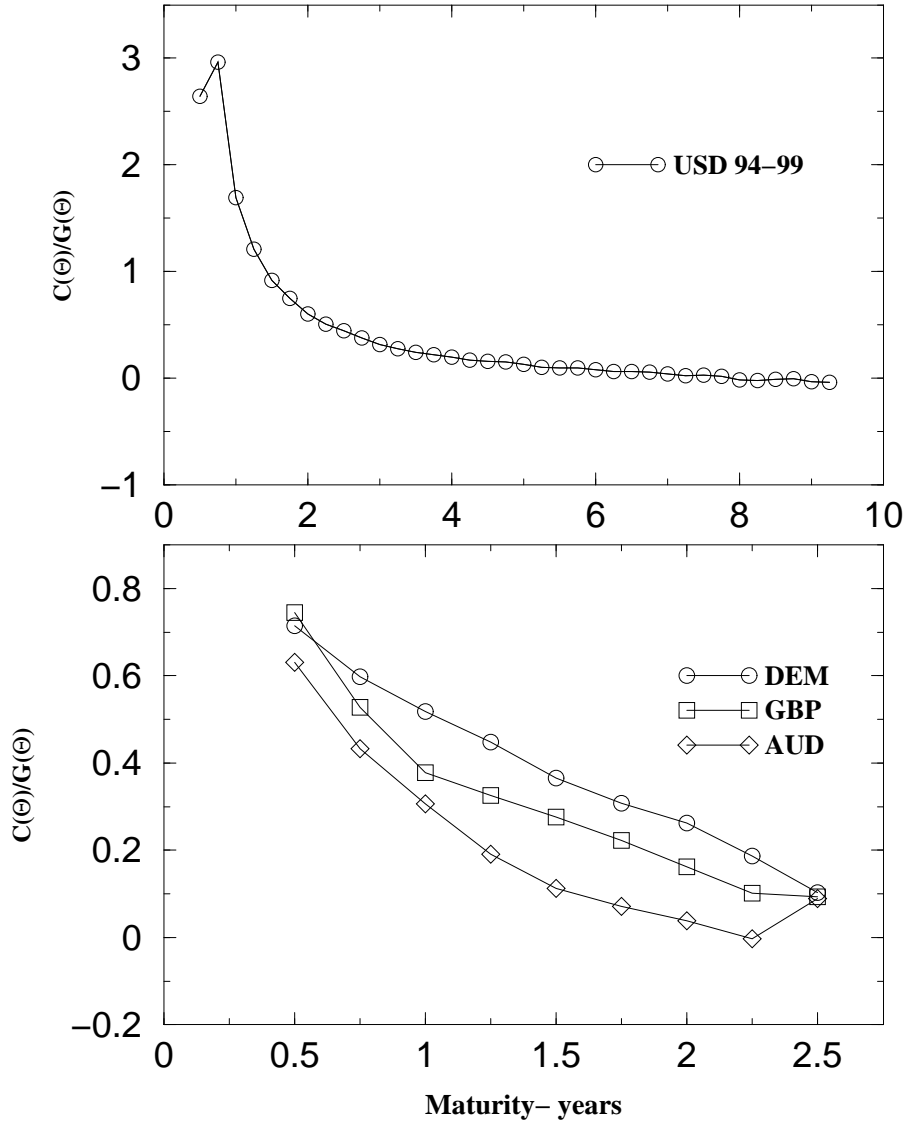


Figure 11: Top figure: The deformation signal to noise ratio: $C(\theta)/G(\theta)$ for the USD 94-99. Bottom figure: the same but now for the currencies GBP, DEM and AUD. First $C(\theta)$ is determined from Eq. (4.18), using the empirical average FRC and the response function. Then $G(\theta)$ is calibrated to the empirical FRC volatility using Eq. (4.19). From Eq. (4.11) we see that the signal to noise ratio provides a relative measure of the spot and noise contributions to a deformation increment. These figures demonstrate that the USD has a much stronger signal to noise ratio than the other currencies.

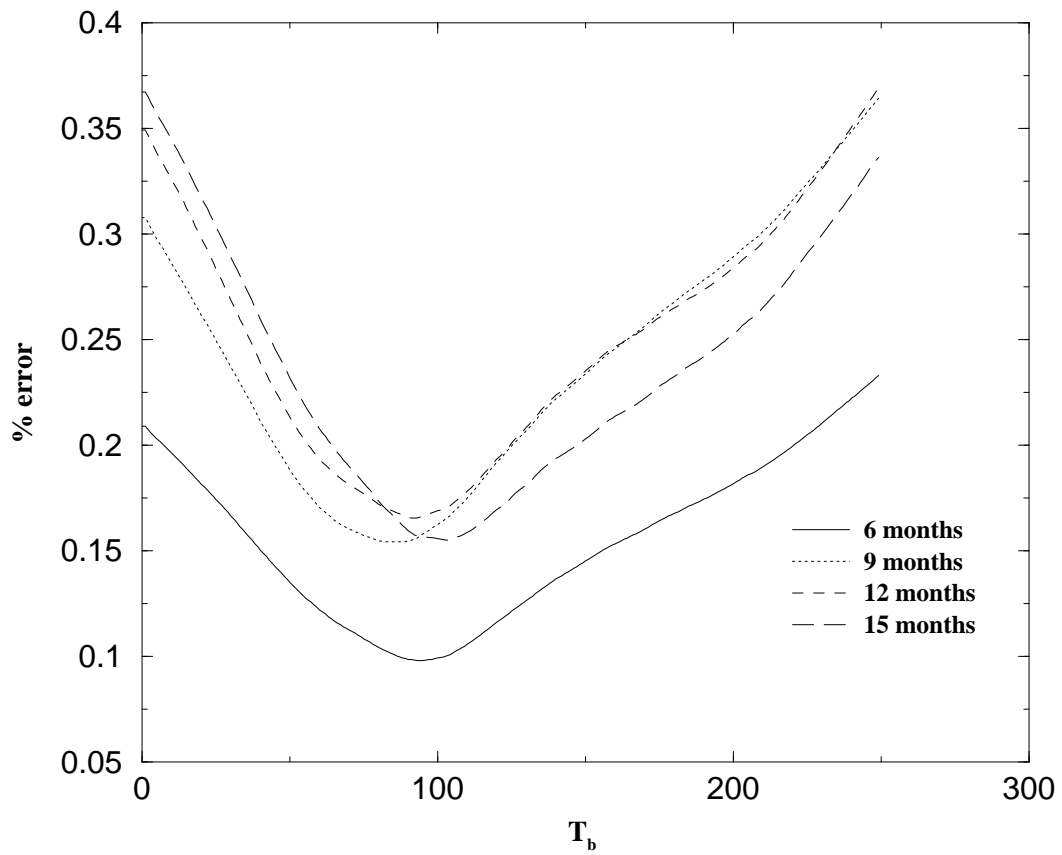


Figure 12: Plot the LHS of Eq. (5.2), against the parameter T_b (in trading days), where for the simulation of $b(t)$ we have used the FW model, Eq. (4.16): for USD 94-99. This figure demonstrates the clear presence of a 100 trading day timescale in the USD FRC dynamics.

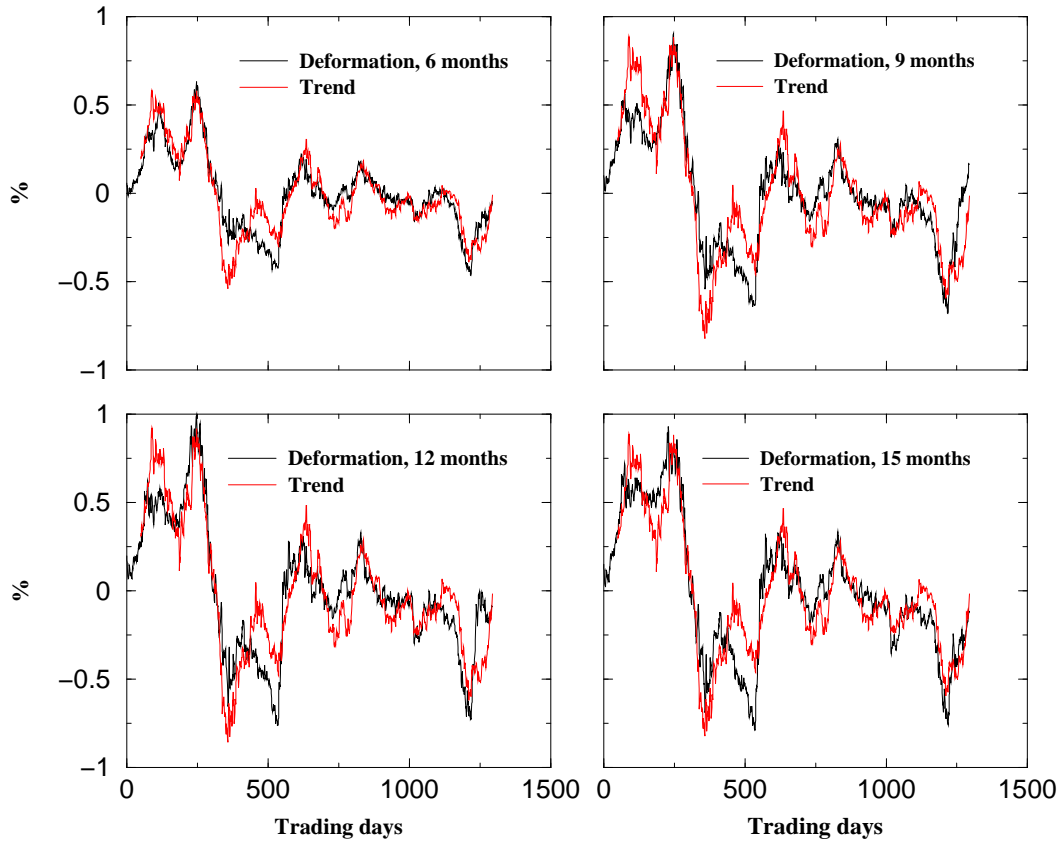


Figure 13: Comparison for USD 94-99, of the empirical deformation process and the scaled anticipated trend, $C(\theta)b(t)$, where $b(t)$ is calculated using the FW model, Eq. (4.16), with $T_b = 100$ days as suggested by the minimum of figure 12. This figure demonstrates a striking correlation between the empirical deformation process and the anticipated trend.

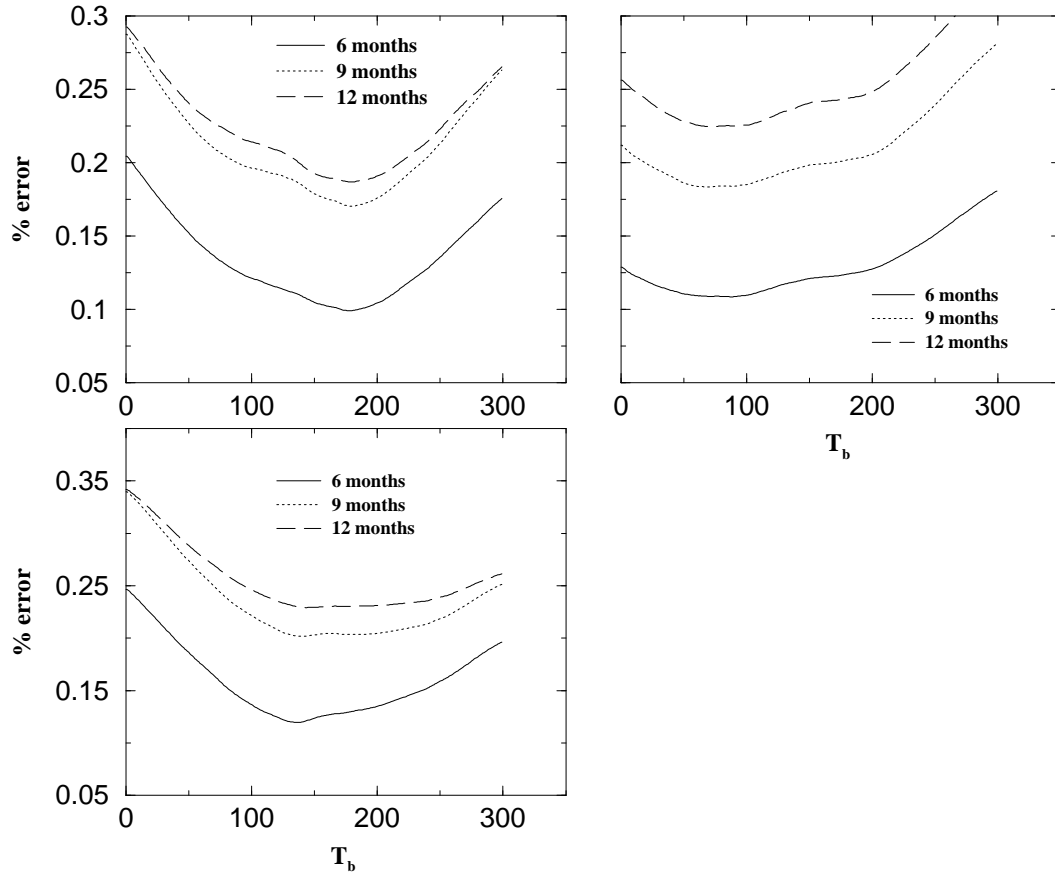


Figure 14: Top left: Same as for figure 12 but now for the GBP. Top right: for the DEM. Bottom left: for the AUD. These figures demonstrates the same qualitative features as found in figure 12 for the USD. Here the minimums are not as well defined. This is expected due to the weaker signal to noise ratio shown in figure 11.

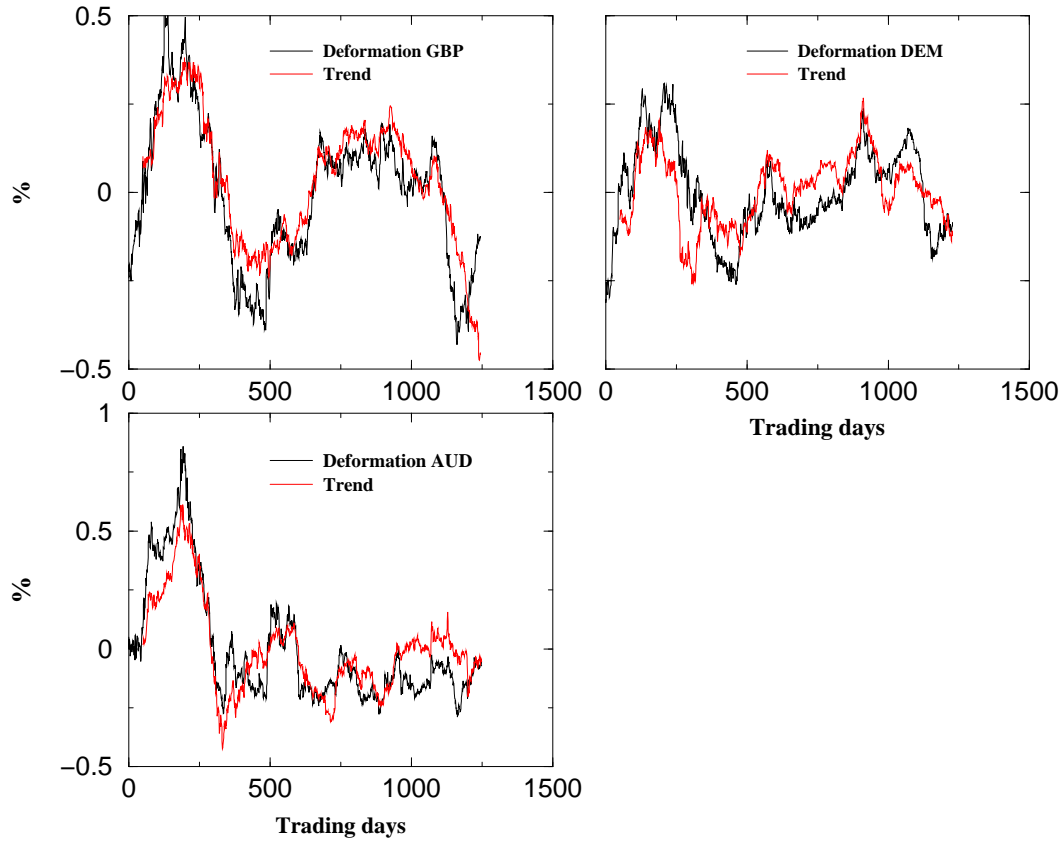


Figure 15: Top left: Comparison for GBP, of the empirical deformation process and the scaled anticipated trend, $C(\theta)b(t)$, where $b(t)$ is calculated using the FW model, Eq. (4.16), with $T_b = 175$ days as suggested by minimum of figure 14. We have used the 6 month maturity. Top right: the same but now for the DEM with $T_b = 100$ days. Bottom left: the same but now for the AUD with $T_b = 130$ days. These figures demonstrate a clear correlation between the empirical deformation process and the anticipated trend. The correlation is not as striking as for the USD due to the lower signal to noise ratio shown in figure 11.

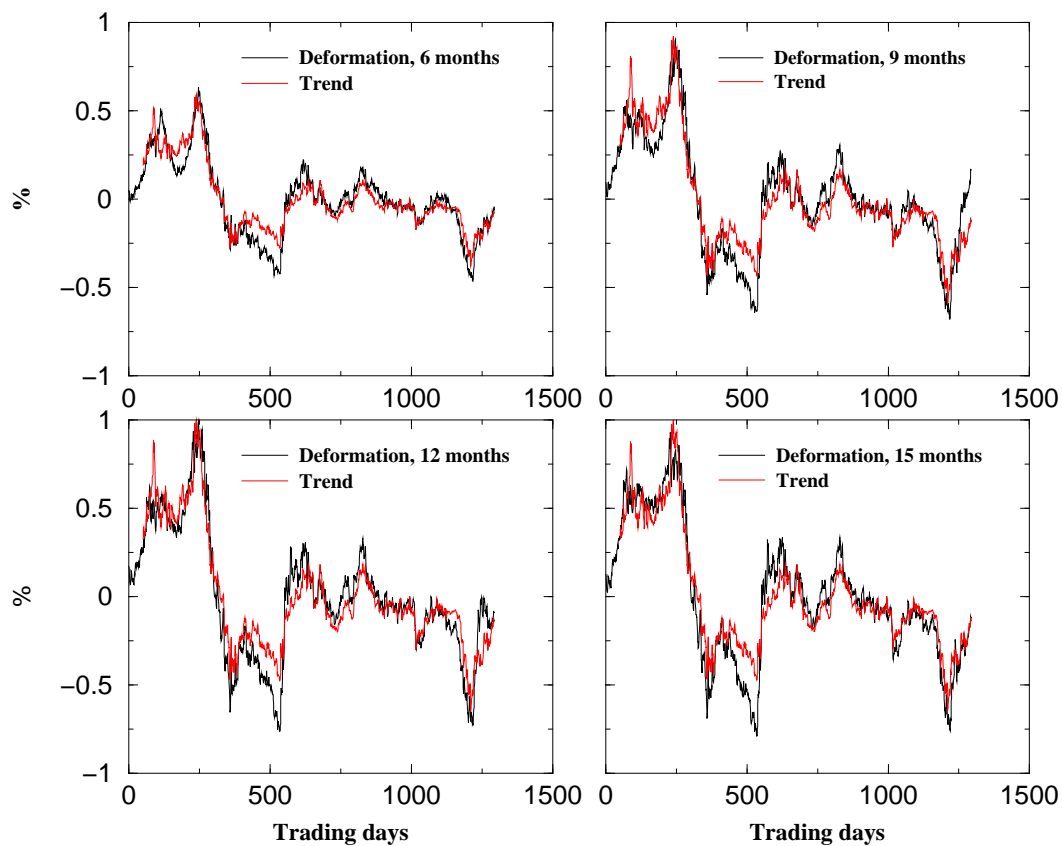


Figure 16: Comparison for USD 94-99, of the empirical deformation process and the scaled anticipated trend, $C(\theta)b(t)$. In this case $b(t)$ is calculated using the OU model, Eq. (4.15), with $\lambda_b^{-1} = 100$ days, while $C(\theta)$ is calibrated to the FRC volatility, Eq. (4.19), where $G(\theta)$ has been set to zero (2 factor model). This figure demonstrates an especially spectacular correlation between the empirical deformation process and the anticipated trend.

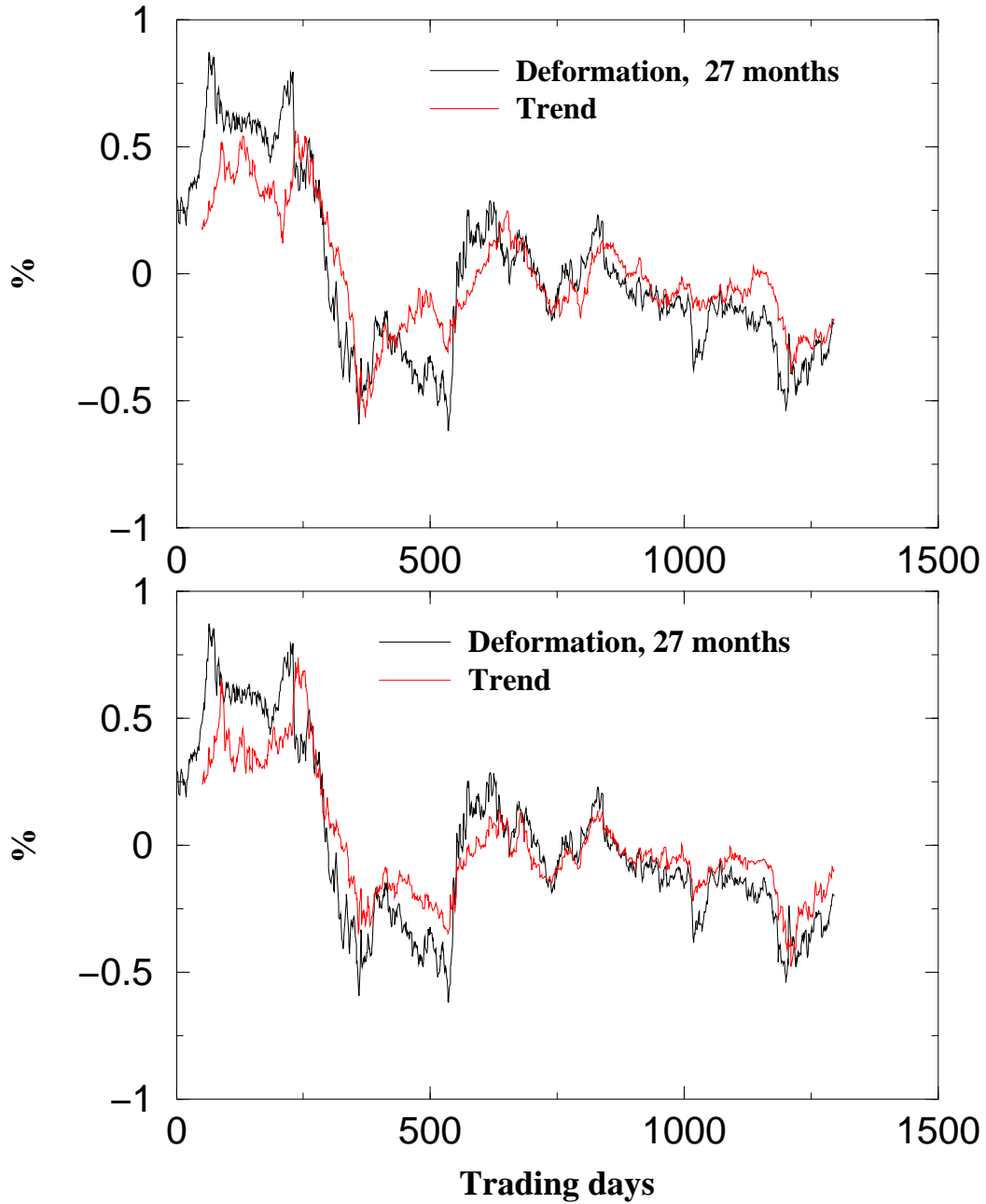


Figure 17: Top Figure: the same as for figure 13 but now for a maturity of 27 months. Bottom Figure: the same as for figure 16 but also now for a maturity of 27 months. This figure demonstrates that the correlation between the empirical deformation and anticipated trend persists even 2 years forward of the spot.

References

- [1] J. Hull (1997), *Options, futures and other derivative securities*, Prentice-Hall.
- [2] J.P. Bouchaud and M. Potters, *Theory of Financial Risk*, (Aléa-Saclay, Eyrolles, Paris, 1997). Available at: <http://www.science-finance.fr>
- [3] see the reprints in: Lane Hughston (ed.) (1997) *Vasicek and beyond*, Risk Publications.
- [4] J.P. Bouchaud, N. Sagna, R. Cont, N. ElKaroui, M. Potters, “Phenomenology of the interest rate curve”, cond-mat/9712164, to appear in Applied Mathematical Finance (1999). J.P. Bouchaud, N. Sagna, R. Cont, N. ElKaroui, M. Potters, RISK Magazine, July 1998. Both available at: <http://www.science-finance.fr>
- [5] R. Cont, “Modeling Term Structure Dynamics: An Infinite Dimensional Approach”, to appear in I.J.T.A.F. (1999). Available at: <http://www.cmap.polytechnique.fr/~rama/>
- [6] J.M. Moraleda, A. Pelsser, “Forward vs. Spot Interest Rate models”, Working Paper, Erasmus University, Rotterdam (1997).
- [7] B. Piccinato, G. Ballocci, M.M. Dacorogna and R. Gencay, “Intraday statistical properties of Eurofutures” (1998). Available at: <http://www.olsen.ch>
- [8] D. Heath, R. Jarrow and A. Morton, “Bond pricing and the term structure of interest rates: A new methodology for contingent claim valuation”, *Econometrica* **60**, (1992), 77-105.
- [9] J. Hull and A. White, “Numerical procedures for implementing term structure models II: two-factor models”, *Journal of Derivatives*, **Winter**, (1994), 37-48.
- [10] C. Chiarella and O. Kwon, “Classes of Interest Rate Models Under the HJM Framework”, Working Paper, School of Finance and Economics, UTS (1999). To be available at: <http://www.bus.uts.edu.au/fin&econ/qf/>